Ocean Modelling 161 (2021) 101791

Contents lists available at ScienceDirect

Ocean Modelling

journal homepage: www.elsevier.com/locate/ocemod

Coastal circulation and water transport properties of the Red Sea Project lagoon

Peng Zhan [a], George Krokos [a], Sabique Langodan [a], Daquan Guo [a], Hari Dasari [a], Vassilis P. Papadopoulos [b], Pierre F.J. Lermusiaux [c], Omar M. Knio [a], Ibrahim Hoteit [a,*]

[a] Division of Physical Sciences and Engineering, King Abdullah University of Science and Technology, Thuwal, Saudi Arabia
[b] Hellenic Centre for Marine Research, Anavissos, Greece
[c] Department of Mechanical Engineering, Massachusetts Institute of Technology, Cambridge, MA, USA

ARTICLE INFO

Keywords:
The Red Sea Project
Lagoon
Residence time
Lagrangian coherent structures
Coastal
Transport

ABSTRACT

The Red Sea Project (RSP) is based on a coastal lagoon with over 90 pristine islands. The project intends to transform the Red Sea coast into a world-class tourist destination. To better understand the regional dynamics and water exchange scenarios in the lagoon, a high-resolution numerical model is implemented. The general and tidal circulation dynamics are then investigated with a particular focus on the response of the lagoon to strong wind jets. Significant variations in winter and summer circulation patterns are identified. The tidal amplitude inside the lagoon is greater than that outside, with strong tidal currents passing over its surrounding coral reef banks. The lagoon rapidly responds to the strong easterly wind jets that occur mainly in winter; it develops a reverse flow at greater depths, and the coastal water elevation is instantly affected. Lagrangian particle simulations are conducted to study the residence time of water in the lagoon. The results suggest that water renewal is slow in winter. Analysis of the Lagrangian coherent structures (LCS) reveals that water renewal is largely linked to the circulation patterns in the lagoon. In winter, the water becomes restricted in the central lagoon with only moderate exchange, whereas in summer, more circulation is observed with a higher degree of interaction between the central lagoon and external water. The results of LCS also highlight the tidal contribution to stirring and mixing while identifying the hotspots of the phenomenon. Our analysis demonstrates an effective approach for studying regional water mixing and connectivity, which could support coastal management in data-limited regions.

1. Introduction

The Red Sea is regarded as a natural treasure with its abundant, thriving coral reef ecosystems, and the unique marine conditions they thrive in, including extreme temperature and salinity (Carvalho et al., 2019). The Red Sea Project (RSP) is located in northwestern Saudi Arabia on the Red Sea coast (https://www.theredsea.sa). The development of the project is spread over an area of about 1,600 km^2 and encompasses more than 90 pristine islands in a lagoon-like basin. The basin is bordered by massive onshore barrier reefs and small islands, whose steep shoreline cliffs cut sharply into the sea. These natural barriers partially isolate the basin from the surrounding sea, with limited water exchange occurring through narrow channels and shallow banks over the reefs (Fig. 1).

At the RSP lagoon, northwesterly winds dominate over the sea throughout the year (Langodan et al., 2017b). However, the wind regime from the land is variable because of the smaller valleys that cut through nearby mountain ridges and cause strong, episodic easterly jets (Jiang et al., 2009), especially in winter. The regional oceanic circulation features a northward boundary current along the Saudi coast (Yao et al., 2014b,a) and frequent eddies that are more active in winter (Zhan et al., 2014, 2016, 2018, 2019). These eddies and boundary current events can affect the regional circulation outside the lagoon and potentially influence the internal flow. Circulation over reefs can be driven by several mechanisms, including tides, wind, buoyancy effects, and waves (Andrews, 1990; Lentz et al., 2016b, 2017). Wave breaking occurs on the forereef, which causes a local increase in water level and a pressure gradient that drives cross-reef flows. This is an important force for small lagoons with offshore sizes of less than 3 km (Symonds et al., 1995; Kraines et al., 1998; Lugo-Fernández et al., 2004; Lowe et al., 2009; Lentz et al., 2016a; Guo et al., 2021). However, for larger lagoons, the circulation is mainly driven by winds, tides, and buoyancy effects (Balotro et al., 2003; Monismith et al., 2006; Umgiesser et al., 2014; Montaño-Ley and Soto-Jiménez, 2019). An estimate of the wave-driven flow across the forereef of the RSP lagoon using Lentz et al.

---

[*] Corresponding author.
E-mail address: ibrahim.hoteit@kaust.edu.sa (I. Hoteit).

https://doi.org/10.1016/j.ocemod.2021.101791
Received 18 June 2020; Received in revised form 1 March 2021; Accepted 16 March 2021

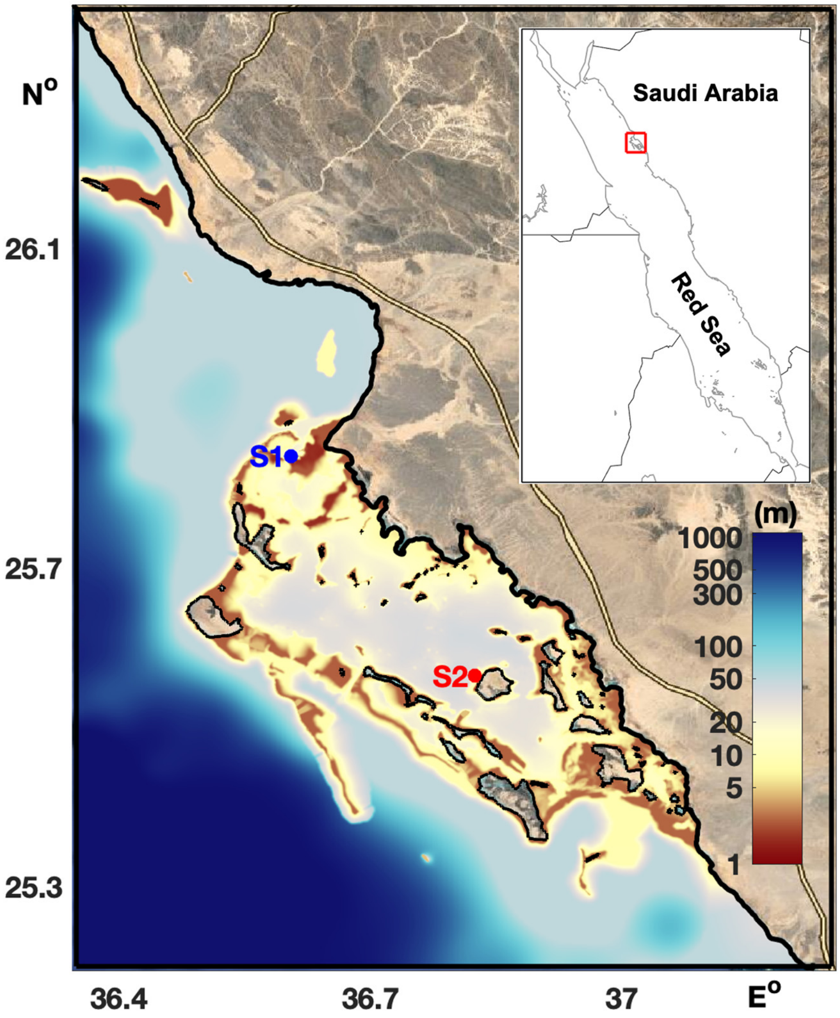

Fig. 1. Domain of simulation with bathymetry in color and islands and coastlines demarcated in black. The light gray patches indicate the shallow areas occupied by coral reefs, whereas the blue and red dots indicate the locations of two *in* − *situ* observation sites.

(2016b)'s idealized model suggests that the cross-reef velocity is of less than 0.05 m/s, and this has been verified by an ADCIRC wave-coupled model (not shown). Therefore, the wave effects are considered to be small and presumably do not have a significant impact on the circulation of the RSP lagoon, whose offshore front is typically more than 30 km away from the coastline.

The variability in water fluxes through the inlets determines the lagoon flushing rates and influences the water quality, salt (brine), and heat balance, and ecosystem (Lowe et al., 2009; Tartinville et al., 1997; Umgiesser et al., 2014; Doshi et al., 2019). The residence time (RT) is defined as the amount of time a fluid parcel remains in a region before crossing a particular boundary (Cavalcante et al., 2012). Understanding RT is vital to characterize the conditions of the marine ecosystem and evaluate the potential consequences of human activities within a water body. It is also a key factor in determining the rate at which biologically important components of marine species, such as nutrients and larvae, are exchanged with the open ocean. Residence time further controls a variety of key processes in coastal lagoons, including the transport and dispersal of various water masses (Oliveira and Kjerfve, 1993; Cerralbo et al., 2016), water renewal (Balotro et al., 2003; Umgiesser et al., 2014; Georgiou et al., 2020), and coastal biomass evolution (Tartinville et al., 1997; Yahel et al., 1998).

The RSP aims to develop a world-class tourism project, and the lagoon, recognized for its ecological and economic importance, has been declared a conservation zone. In such coastal systems, the distribution and transport of important water properties (temperature, salinity, and concentration of nutrients, larvae, and pollutants) as well as of life forms incapable of locomotion, critically depend on the circulation patterns and possible oscillations due to tides or transient winds that could generate turbulence and mixing (Csanady, 1982). Till date, knowledge about the regional circulation is limited. The unique dynamics of the RSP lagoon, its response to atmospheric conditions, and the role of circulation in structuring its water exchange and renewal are poorly understood owing to the lack of adequate observations. In this study, we address this gap by investigating the hydrodynamics of the region and RT of water and by discussing their seasonal and spatial variability, based on the results of state-of-the-art high-resolution numerical models and methods. The goal is to improve our understanding of the spatial and temporal extent of coastal processes in the RSP lagoon. The manuscript is organized as follows: Section 2 briefly describes the numerical models and methods. Section 3 outlines the general and tidal circulation patterns in the RSP lagoon. The RT is estimated and discussed in Section 4, including the analysis of Lagrangian coherent structures (LCS) in Section 5. A discussion and summary of the main results are provided in Section 6.

2. Models and methods

A high-resolution MIT general circulation model (MITgcm) (Marshall et al., 1997) was implemented to simulate the circulation in the coastal region of the RSP, ranging from 36.35° E to 37.25° E and

$25.2^{\circ}N$ to $26.4^{\circ}N$. The model uses spherical coordinates with a horizontal resolution of approximately 75 m and 50 vertical z-levels, whose thickness gradually increases from 0.5 m at the surface to 180 m at the bottom. This resolution was selected to handle the extremely complex topography and jagged coastlines. Daily temperature, salinity, and horizontal velocity fields at the southern and western open boundaries were nested within a 1-km model that was configured to simulate the general circulation of the entire Red Sea ((Hoteit et al., 2021) an updated version of that implemented by Yao et al. (2014a,b)). The entire Red Sea model was forced with a 5-km Weather Research Forecast (WRF) product (Viswanadhapalli et al., 2017), downscaled from the ERA-Interim products of the European Centre for Medium-Range Weather Forecasts (ECMWF) (Dee et al., 2011) and further assimilated the available remote sensing (Quick Scatterometer, Windsat and ASCAT, and geostationary satellites) and $in-situ$ (synoptic stations, Metar, ship, Rawinsonde and pilot balloon) datasets in the region. To ensure that the variations in mean water elevations in the coastal model are consistent with the 1-km Red Sea model, the normal velocities at the southern and western open boundaries were adjusted to match the exact volume flux of the regional Red Sea model. The K-profile parameterization (KPP) scheme (Large et al., 1994) was used to consolidate strategies for a variety of unresolved processes involved in vertical mixing. The bottom drag was estimated using the no-slip scheme, in which a friction term is computed in the grid cell above the bottom and its magnitude is proportional to the vertical viscosity (Griffies and Hallberg, 2000). Meanwhile, the quadratic bottom drag scheme (coefficient = 0.01) was applied to the no-slip condition, as a function of the velocity immediately above the topography, with the specified coefficient being the same order as that estimated by Lentz et al. (2017).

For the RSP coastal model, barotropic tidal forcing was applied at the boundaries by prescribing the amplitudes and phases at 1-hour intervals. The tidal parameters were extracted from the inverse barotropic tidal model, TPXO 7.2, for the Indian Ocean (Red Sea) (Egbert et al., 1994), including eight major tidal components of semidiurnal and diurnal frequencies (M2, S2, N2, K2, K1, O1, P1, and Q1). This model is driven by hourly surface wind, air temperature, specific humidity, precipitation, and downward shortwave and longwave radiation values generated from a 3-km WRF product. This was carried out using an approach similar to that used to develop the 5-km regional Red Sea reanalysis. The surface fluxes, including the net freshwater and heat fluxes, as well as surface wind stress were calculated using the bulk formula from the above-listed atmospheric state variables.

An accurate representation of the seabed topography, which is bordered by abundant coral reefs and islands, was necessary to successfully model the circulation in the region. In and around these reefs, which exhibit steep edges and sudden drop-offs, the water depth can vary dramatically. To generate a fine-scale high-resolution bathymetry of the model domain, data from various sources were collected, cross-validated, and merged. This data included measurements from six $ad-hoc$ cruises operated in the lagoon, the latest version of the General Bathymetric Chart of the Oceans (Ioc, 2008), and remotely sensed high-resolution images. Our exhaustive research yielded the most accurate and complete representation of the coastlines and near-shore bathymetry, with more than 200 islands, coastal shelves, and shallow reefs being now meticulously in the domain (Fig. 1).

We analyzed the period between February 2017 and April 2018. The regional assimilative WRF model outputs were validated and extensively used in regional climate studies (Langodan et al., 2017b; Viswanadhapalli et al., 2017; Langodan et al., 2017a). The 1-km Red Sea model has been validated against independent observations of conductivity, temperature, and depth across the Red Sea (George Krokos, personal communication, May 16, 2019), and satellite sea surface height (SSH) and sea surface temperature (SST) data (Toye et al., 2017), providing satisfactory boundary conditions for the nested model. The nested model was validated against $in-situ$ observations of water elevation and temperature collected between November 2017 and January 2018 at the two stations shown in Fig. 1. A comparison between the outputs of the model and the observed elevations is shown in Fig. 2(a–d), and the simulated seawater temperature is compared with the Level-4 Global 1-km Sea Surface Temperature (G1SST) dataset (Chao et al., 2009) and $in-situ$ observations (Fig. 2e–g). The root mean square error (RMSE) in water elevation is in the order of centimeters, and the RMSEs in temperature are less than 1 °C (Fig. 2). In general, the model results agree with available observations, notwithstanding some inevitable discrepancies, and the comparative data limitations due to the paucity of $in-situ$ observations. The non-assimilative model used here may not reproduce the full flow structures in the RSP region, particularly when the adjacent open sea is subject to random eddies (Zhan et al., 2014, 2015). However, this should not affect the findings of this work in term of the general circulation dynamics of the region, as the primary seasonal circulation scenarios and key dynamics are validated based on the presented model-observation comparisons.

The Lagrangian trajectories of passive particles are simulated using the connectivity modeling system (CMS) (Paris et al., 2013). The CMS is a probabilistic model of particle dispersal based on a stochastic Lagrangian framework. Driven by the velocity fields from the MITgcm outputs, the CMS computes the particle locations and tracks of their pathways following a multigrid approach. The CMS provides a Lagrangian description of oceanic advection and dispersion. It is a useful tool for studying concentrate discharges (Zhan et al., 2015), biological connectivity among various coral reef complexes at the coastal scale (Nanninga et al., 2015; Lindo-Atichati et al., 2016), basin scale (Raitsos et al., 2017), and cross-basin scale (Wang et al., 2019).

The fate of tracers in the ocean is closely related to emerging patterns commonly referred to as LCS (Peacock and Dabiri, 2010), which are identified as ridges of the finite-time Lyapunov exponent (FTLE) fields (Shadden et al., 2005) (Appendix B). The LCS is a Lagrangian diagnostics that is widely used to study the transport and mixing processes of oceanographic tracers. It can delimit regions of whirls, stretching, or the contraction of tracers (Ottino, 1989; Haza et al., 2016) by representing the material boundaries that separate different regions by particle movement (Duran et al., 2018). The LCS is known to correspond well with major structures, such as filaments, fronts, and spirals, which appear in the geophysical and bio-geochemical tracer fields (Olascoaga et al., 2006, 2008; Beron-Vera and Olascoaga, 2009; Nencioli et al., 2011; Gough et al., 2019). The code used to compute FTLE was developed in collaboration between LOCEAN (F.d'Ovidio) and CLS and is available at https://anaconda.org/fbriol/lagrangian.

3. Coastal circulation in the RSP lagoon

3.1. General circulation

According to seasonal variations in SST of the region and the northern Red Sea (Yao et al., 2014b,a) that reaches lowest and highest annual range, January–February, and August–September are selected as the representative months for the winter and summer scenarios, respectively. Accordingly, all analyzed data for the two seasons is extracted from these months.

The average seasonal circulation in the RSP region exhibits different patterns in winter and summer, as shown in Fig. 3(a and b), with the SST displayed in color and superimposed by the volume transport integrated over the upper 20 m. Outside the lagoon, strong northwestward currents persist in both seasons at speeds exceeding 0.5 m/s on the surface, a similar feature has been found from the AVISO monthly averaged geostrophic velocities (not shown). These currents generate a retroflection that extends and enters the lagoon from the north. (Note that the arrows inside the lagoon are in white and their magnitudes are plotted four times larger than those outside the lagoon, for better visibility.) In winter, the mean flow inside the lagoon is usually weak. This is because wind jets that occur in the winter months can force the water northwestward and therefore compensate the aforementioned

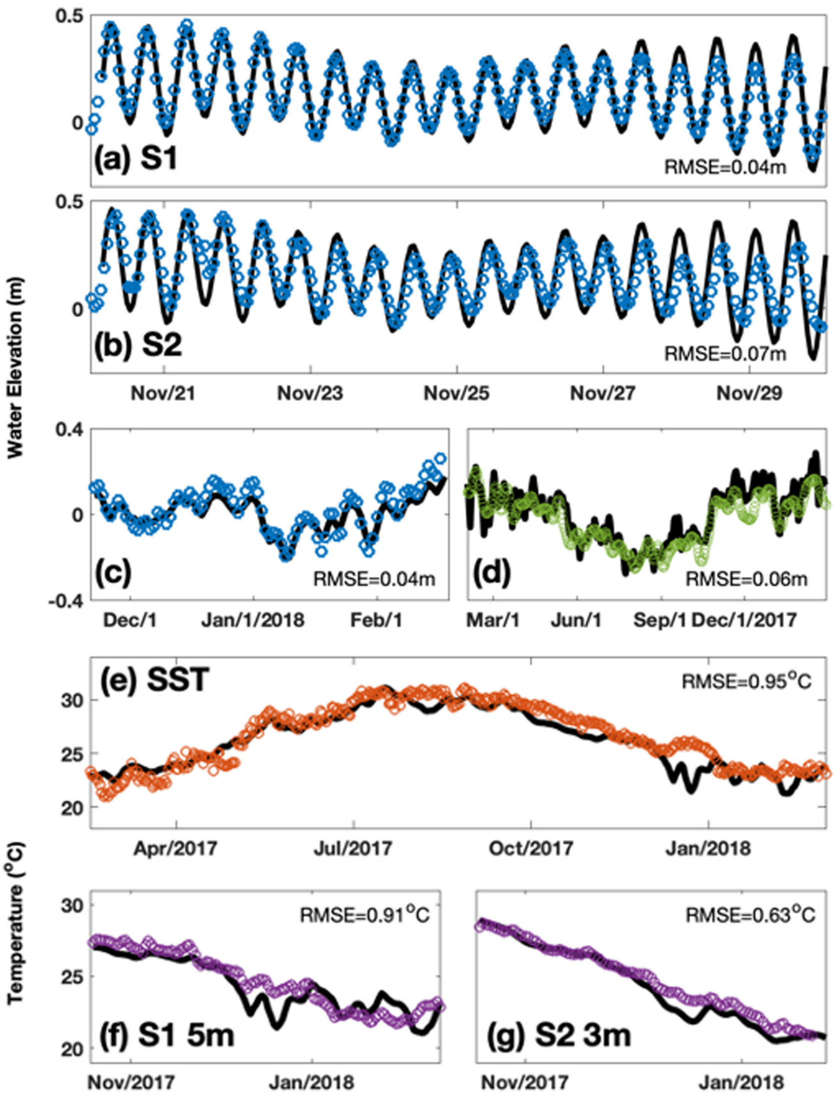

Fig. 2. Comparison of simulated water elevation (black curves) with observations (colored dots) at difference locations and frequencies: (a) hourly data at S1, (b) hourly data at S2, (c) daily averaged data at S2, (d) daily and domain average SSH data from AVISO (processed by SSALTO/DUACS and distributed by AVISO+ (https://www.aviso.altimetry.fr) with support from CNES). Comparison of simulated SST (black curves) in comparison with observations (color dots) of G1SST averaged over the lagoon, (e) $in-situ$ measurements at S1 (f) and S2 (g), respectively.

southeastward currents (details are discussed in Section 3.3). In summer, currents from the north flow toward the central and southeastern lagoon and form a counterclockwise circulation, although its shape is highly deformed. Also, a noticeable difference in summer is marked by a coastal branch that is bifurcated from the inflow. This branch extends along the curved coastline and gradually decays toward the shallow waters among the southern offshore islands. The average flows exit the lagoon through the western and southern outlets in summer. The majority of these outlets are obstructed by coral reefs, with depths of about 2 m except for a few deeper channels (Fig. 1).

The mean circulation inside the lagoon is weaker than that outside the lagoon; however, the SST exhibits greater variability. The SST inside the lagoon ranges between approximately 20 and 32 °C over a year, varying much more than the open sea SST, which varies about 24 and 30 °C. This is clearly illustrated by the seasonal temperature averages in the cross section plotted in Fig. 3(c and d). The winter scenario is characterized by cold water inside the lagoon with the isothermal doming to the surface, whereas in summer, the central lagoon is filled with warm water throughout the column and exhibits weak stratification. A close examination of Fig. 3(c and d) shows that the water is more confined within the lagoon in winter, whereas in summer, the northern part of the lagoon hosts water intruded from the north. This wide range of seasonal variability is attributed to the limited heat capacity of the lagoon water, which is subjected to intense seasonal variations of the heat flux (not shown). The mean SST distribution in the central lagoon coincides with the edges marked by the arrows, indicating a larger volume transport. This suggests that the water is trapped by the currents with moderate exchange with the ambient water.

3.2. Tidal currents

Tidal currents in the Red Sea are generally weak, with an average speed of less than 0.1 m/s (Madah et al., 2015; Guo et al., 2016); however, they can be amplified in shallow coastal areas. The results of a harmonic analysis suggest that the dominant tidal signal is associated with the semidiurnal tides; in particular, the M2 component, which exhibits a 12 h 25 min periodicity. The amplitude and phase of the M2 tidal constituent are shown in Fig. 4(a). Owing to the reef topography, the inner lagoon exhibits a greater amplitude at the coast compared with that in the open sea. The tide propagating from the south contacts the outer reef almost simultaneously and is then largely

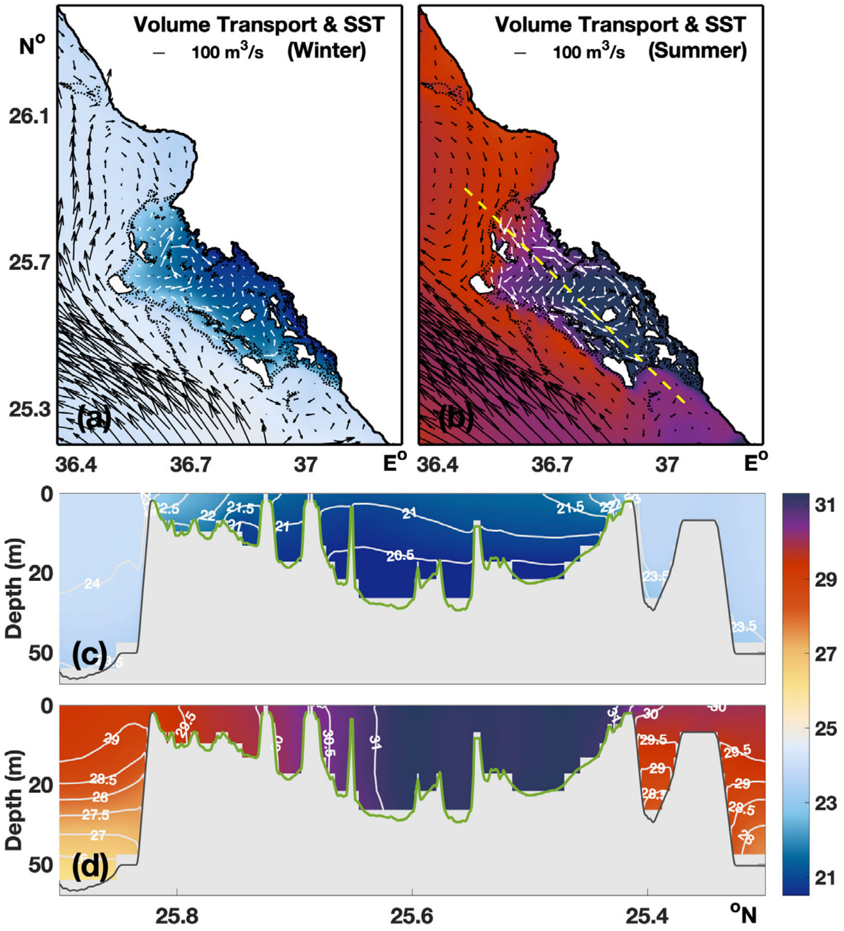

Fig. 3. Seasonally averaged volume transport (in arrows) of the upper 20 m superimposed on the SST (in color): in (a) winter (b) summer. The arrows inside the lagoon are colored in white and their magnitude are plotted four times larger than those outside the lagoon for better visibility. The seasonally averaged temperature in winter and summer at the cross section (marked by the dashed line in b) is illustrated in (c) and (d). The color bar specifies the temperature in units of °C.

obstructed by the shallow reef banks before entering the lagoon. It takes approximately 6–8 min to pass through. The elevation inside the lagoon is isochronous despite the presence of several scattered islands.

The magnitudes of the M2 surface tidal current are shown in color in Fig. 4(b), superimposed with the tidal ellipses. The surface currents are amplified over the shallow reef banks, where the tidal ellipses generally exhibit a higher eccentricity. This suggests that the flood and ebb currents evolve alternately back and forth without a noticeable rotation. This is also reflected by the typical snapshots of the flood and ebb tides shown in Fig. 4(c) and (d), respectively. During both periods, the surface current velocity reaches 0.5 m/s at the reef banks, which is at least five times stronger than that inside the lagoon. During the flood period, a large gradient in elevation appears between the inside and outside of the lagoon, and the tidal currents flood into the lagoon over all of the surrounding reef banks and inlets. During the ebb period, however, the water mainly returns to the open sea through the western and southern reefs, with fairly limited outflow to the north.

Because the RSP lagoon is shallow, it is particularly responsive to heating and cooling processes; warming and cooling are evident even over diurnal time scales. The diurnal variation in the average SST averaged inside the lagoon ranges between 0.4 to 0.8 °C. In addition to the variations imposed by atmospheric forcing, the warmer or colder water from the open sea can be carried by flood or ebb currents depending on the phase. This may amplify or suppress the daily variations in the water temperature inside the lagoon, particularly for water in the vicinity of the surrounding reefs.

3.3. *Response to strong wind jets*

The hydrodynamics within the RSP lagoon are highly responsive to temporal wind variations. Analysis of the wind regime over the region suggests that the area is dominated by northwesterly winds; however, strong episodic easterly wind jets from the mountain gaps occur in the winter months. Significant changes in the circulation patterns can occur within a few days in response to a strong wind event, as the currents adjust to the geostrophic equilibrium for periods in the order of f^{-1} (Csanady, 1982).

The example in Fig. 5 highlights the response of the lagoon water to strong wind jets. Under normal atmospheric conditions with northwesterly winds (Fig. 5a), the daily average surface currents flow southeastward (Fig. 5c). A band of coastal water is cooler because of the shallow topography and its physical isolation from the outer relatively warmer water. The northwesterly wind generates a downwind flow in the upper layers (Fig. 5e) and leads to a higher water elevation toward the southeast lagoon (not shown). This induces a surface-slope pressure gradient, which in turn tends to create a counteracting current at deeper depths of the lagoon (Fig. 5e), as has been reported by Mathieu et al. (2002), Andréfouët et al. (2006). After just two days, during which the wind regime shifts into easterly jets at higher speeds (Fig. 5b), the surface currents in the entire lagoon turn and begin to flow westward and northward (Fig. 5d). The surface heat loss inside the lagoon is significantly intensified, following the higher wind speeds over the lagoon and cooling a large fraction of the surface

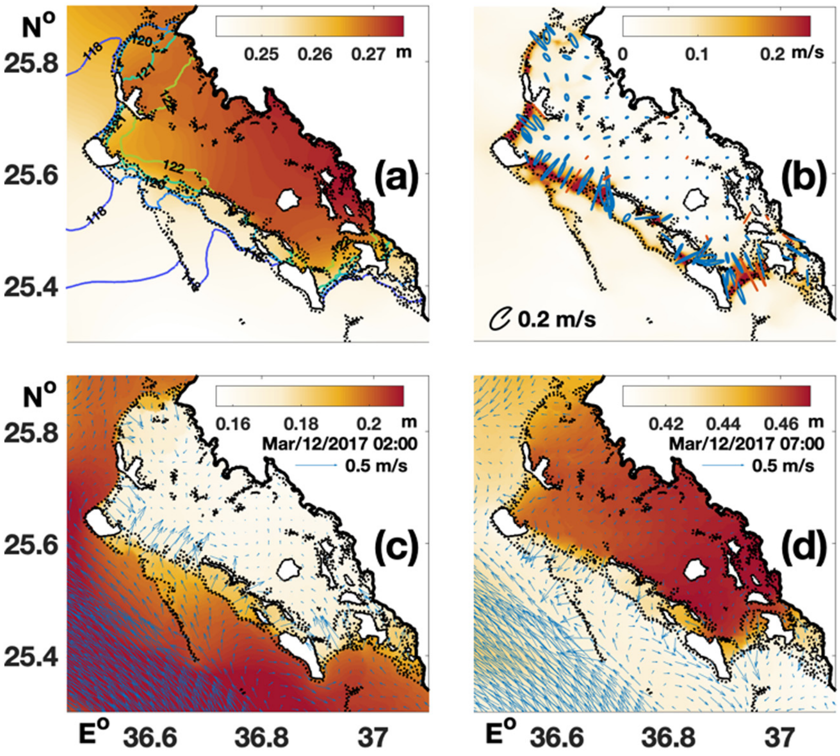

Fig. 4. Distribution of tidal features (M2). (a) Amplitude in color superimposed with phase in contours. (b) Amplitude of tidal current in color superimposed with tidal ellipse, where blue and red represent rotation of clockwise and counterclockwise rotations, respectively. (c) and (d) Snapshots of surface flood currents and ebb currents (arrows) and water elevation (in color) within a tidal cycle, respectively.

water (Fig. 5d). The wind from the land blows surface water offshore, which causes water to pile up against the western reefs and generates a higher mean elevation outside the lagoon (not shown). The reversed northwestward currents at the section could reach a depth of 20 m deep near the coast and reef islands, and are counterbalanced by weak southeastward currents in the deeper layers (Fig. 5f). Similar dynamics with the reversal of the horizontal velocity with depth was observed by Mathieu et al. (2002) in idealized experiments of wind forcing over an enclosed basin, wherein the wind-induced currents in the upper layers were balanced by the returning flows in the lower layers.

A close examination of the variation in coastal elevation reveals a ~10-day oscillation in the winter months, as depicted by the time series of the de-tided elevation in Fig. 6(a, yellow curve). This starts from December and lasts until February, and is reflected also by the larger magnitude of the wavelet scalogram of the elevation (Fig. 6b). This feature is only observed in winter. The particular oscillation correlates with the highly variable offshore component of wind stress over the lagoon (coefficient = 0.46, Fig. 6c). Strong wind jets periodically blow offshore during this period and push water out of the lagoon, which results in a decrease in water elevation (Fig. 6c). When the jets start to moderate, the lagoon rapidly refills almost simultaneously with the wind. This suggests that the mechanism that drives sea level variations within the RSP lagoon differs from that of the central Red Sea coast, which is driven by the along-axis surface wind stress over the southern Red Sea (?) Additionally, the direct wind stress could generate seiches in some restricted or choked coastal lagoons (Gill, 1982; Chapman and Giese, 2019), however, the open outlets all around the RSP lagoon limit its ability to hold water and could only yield a < 2 cm increase in elevation downwind toward the western edge. Such a surface-slope pressure gradient is insufficient to generate seiche waves, and no significant signals of seiches (typical periods ranging from minutes to hours) are observed in the wavelet scalogram.

4. *RT*

The *RT* is a measure of the water-mass retention within defined boundaries (Cavalcante et al., 2012) and is often used as a key hydromorphological element for evaluating water quality (Monsen et al., 2002). The *RT* scale of a lagoon depends on the character and strength of the physical transport processes between the domain of interest and the adjacent seas. In this study, passive particles are released throughout the lagoon at seven different depths (evenly distributed from 0 to 30 m with a 5-m interval ~ 85000 in total per day) and their trajectories are simulated based on hourly three-dimensional velocity fields. The particle trajectories are then used to determine the time at which each particle exits the lagoon, which allows estimation of the spatial distribution of *RT* at different depths. A particle is considered to leave the lagoon when it crosses the boundary, as indicated by the colored edge in Fig. 7(a–h). For those particles initially released near the lagoon edges, the *RT* values are sensitive to the phase of the tide (Monsen et al., 2002). However, this effect was mitigated by averaging the daily *RT* over a two-month period. The particles are released every 24 h, yielding 60 different simulations that are then averaged for each season.

The spatial distributions of 2-month averaged *RT* in winter and summer are illustrated in Fig. 7(a–g). The *RT* values inside the lagoon vary greatly in space and time. The *RT* in winter is generally longer, particularly at deeper layers, with a large fraction of the lagoon water exhibiting more than 90 *days* of *RT*. By comparison, the lagoon water is likely refreshed at a faster rate in the summer. In both seasons, the water entering the lagoon during the flood tide remains near the reefs and leaves the lagoon as soon as the tidal currents reverse. Consequently, the *RT* is much shorter in the vicinity of the surrounding reefs. Meanwhile, the *RT* values near the western and southern boundaries are shorter because the water can be flushed out by the southward

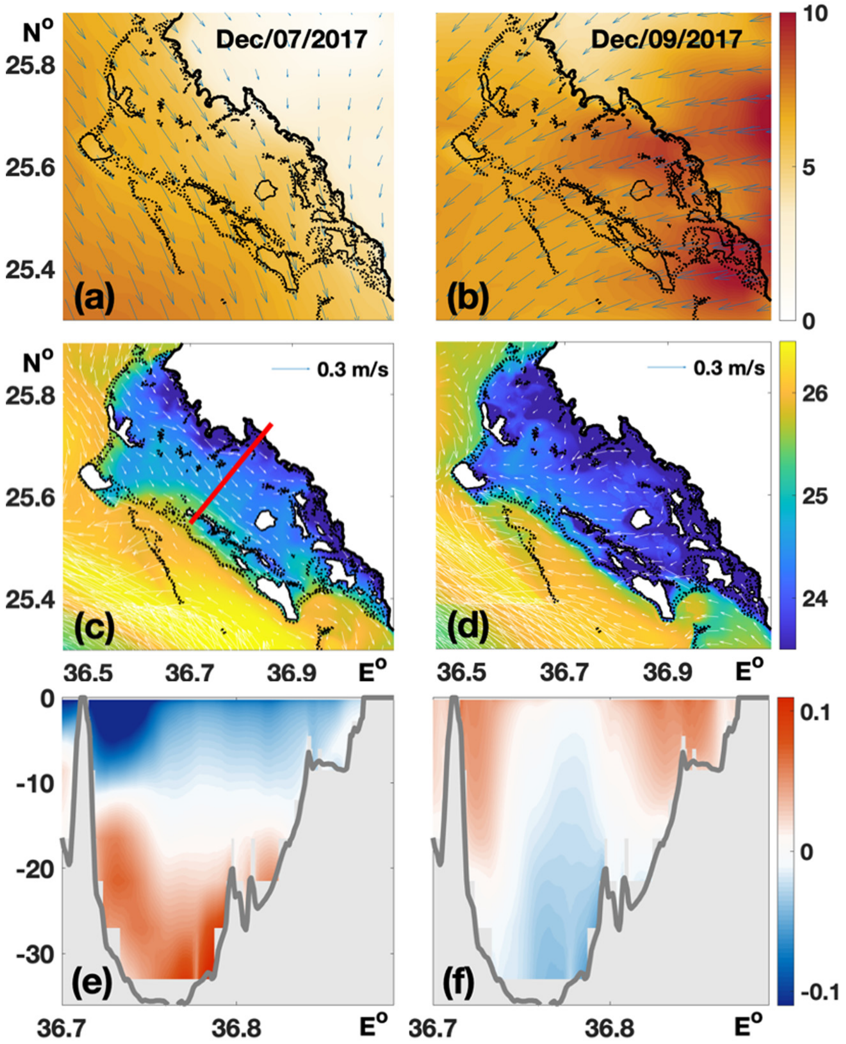

Fig. 5. Daily averaged properties on December 7, 2017 and December 9, 2017, respectively, which represent the atmospheric and oceanic conditions before and after an easterly wind event: (a and b) wind speed (m/s, in color) superimposed with wind vectors, where the color bar specifies the wind speed in units of m/s; (c and d) SST (°C, in color) superimposed by surface currents, where the color bar specifies the temperature in units of °C; (e and f) velocity profiles flowing across the section indicated by the red line in (c), where positive/negative values represent northwestward/southeastward velocities across the section, respectively. The color bar specifies the velocity in units of m/s.

background currents that exit through the western and southern outlets. In contrast, the *RT* values in the central lagoon are much longer, which suggests a relatively weak connection to the open ocean. Another key difference is that the coastal *RT* is considerably shorter in summer compared with that in winter. This is particularly true near the inner cape and bay at $25.7° N$. This is largely caused by the southward background flow along the coast, which occurs only in summer as describe in Section 3.1 (Fig. 3b). In contrast, water appears to be poorly advected by the weaker coastal current in winter. In addition, to diagnose the timescales involved in the water exchange and renewal, we also estimate the percentage of particles that remain in the lagoon. This evolution averaged over different starting times within the seasons are outlined in Fig. 7(i). Particles released in winter generally stay inside the lagoon for much longer. If the percentage left is chosen to be one third of the initial amount, it takes 81 days to decrease to that level in winter, while only 40 days in summer.

5. LCS

LCS have been used to describe and investigate the dispersion of various flow regimes in coastal seas (Lekien et al., 2005; Nencioli et al., 2011; Huhn et al., 2012; Fiorentino et al., 2012; Doshi et al., 2019). Typical features marked by an LCS could be edges of strong currents and eddies, along which the water stretches and molds. The LCS can be represented by the ridges of the forward or backward FTLE, which approximate the repelling or attracting manifolds, respectively (Appendix B). More specifically, nearby water parcels at the end time but on different sides of the backward FTLE ridges have come from disparate origins, whereas regions away from FTLE ridges are relatively quiescent. The backward FTLE ridges tend to attract water parcels in forward time, acting as material barriers to dispersion and delineating pathways for the evolution of passively advected tracers (Beron-Vera et al., 2010), which is most insightful for the purpose of the present study. Attracting LCS associated to backward integration has a direct physical interpretation (D'Ovidio et al., 2004): tracers (chlorophyll, temperature, etc.) spread along these attracting LCS create their typical filamental structures (Lehahn et al., 2007; Calil and Richards, 2010; Bettencourt et al., 2012).

FTLEs provide the integrated effects of the velocity over a given time span. To unveil areas of different stirring features between seasons, FTLEs are computed based on daily vertical-mean velocities over 30 days elapsed backward in time, starting from the end of each simulation. The FTLE of typical months in winter (Jan. 27, 2018 to Feb. 25, 2018) and summer (Aug. 24, 2017 to Sept. 23, 2017) are displayed in Fig. 8. The dark ridges correspond to attracting LCSs, in which water from one side of the ridges does not significantly leak into the

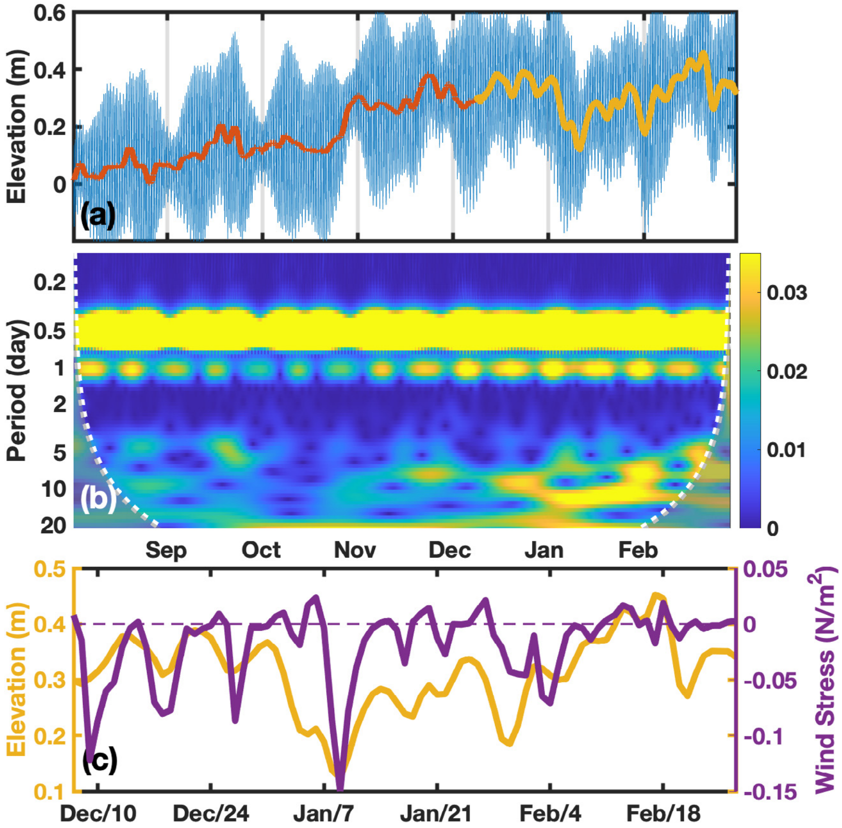

Fig. 6. Elevation at the coastal region inside the RSP lagoon from August 2017 to February 2018. (a) Time series of the simulated hourly elevation (thin blue curve) and the corresponding de-tided signal (thick red and yellow curve). (b) Wavelet scalogram of the hourly elevation time series (namely the blue curve in a). Gray regions outside the dashed white lines delineate the regions where edge effects are significant. (c) Time series of daily averaged elevation at the coast (yellow curve, same as the yellow curve in a) and corresponding wind stress averaged over the RSP lagoon (purple curve). The negative values of the latter indicate that the direction of wind stress is offshore. The period is selected from December 7, 2017 to February 28, 2018.

other side, which indicates manifolds as barriers to material flow. The northern part, marked by dark patches, results from a large aggregation of manifolds. Therefore, they are areas of high deformation and stretching during the 30-day period and water mixes and get advected farther away as the dark patches extend. This is a prominent feature at the northern lagoon in both seasons, largely caused by the high rate of mixing when water flows over and interacts with the shallow topography of the reef complexes. We also stress here the appearance of a clear barrier in both seasons that separates the lagoon from the southwest open sea, despite the strong northwestward current (Fig. 3a and b).

Compared with those in winter (Fig. 9a), more abundant and intense ridges in summer (Fig. 9b) connect the lagoon with the open sea to its northwestern, and, in particular, its southeastern regions. The higher degree of connection indicates rapid water exchange and conforms with the shorter *RT* in summer. Another noticeable disparity is indicated by the white patch at the inner lagoon in winter, versus the curvy orange ridges in summer. As the FTLE can be considered as a skeleton of the connectivity pattern (Hernández-Carrasco et al., 2013), this implies that water of the central the RSP lagoon is relatively quiescent and isolated in winter, and becomes more ventilated in summer. Moreover, in the summer month, darker patches extended to the south of the lagoon suggests noticeable outflow in that region, which is not seen in the winter month.

To illustrate the relationship between the LCS and transport patterns, the same high values of the 30-day FTLE are shown in Fig. 9 appearing as a network of lines, superimposed with locations of passive particles released in the northern, central and southern basins at the beginning of the 30 days. The sequence of particles reveals properties of the dynamics that developed for a wide-range of flows. In the winter months, Fig. 9(a–c), shows a light patch surrounded by dark ridges in the central lagoon indicates that the water mass is likely detained in the central lagoon, with limited connection to the ambient waters. Consequently, the red particles are trapped within the patches without flowing across the surrounding darker barriers and mixing with the blue or green particles released at the northern or southern lagoon, which leads to a significantly longer *RT* (Fig. 7a). The displacement of a fluid parcel is indeed constrained by the LCS transport barriers without noticeable leakage. Because water can flow northward owing to the dominant wind jets during this period, as discussed in Section 3.3, some blue particles exit the lagoon through the northern outlets and move following the ridges, while the rest are retained in the northern lagoon. The large differences in the fates for the proximal initialization indicate a high sensitivity to initial location across the FTLE ridges. By contrast, ridges in summer (Fig. 9d–f) aggregate with each other and fill the entire lagoon, suggesting active exchange and mixing. Under these circumstances, the water mass is more likely to deform and mix with ambient water, as shown by the mingled particles in the lagoon. The background flow in summer is generally southeastward; therefore, the ridges extend to the open sea through the southern outlet, after which all of the green particles and some of the red particles are flushed out of the lagoon. This channel acts as the main exit for the outflow in summer; therefore, it is conducive to a shorter *RT*. After exiting, some of the green particles are entrained by the strong northwestward current following the FTLE ridges. In general, the tracer evolves very tightly following the evolution of the LCS, which explicitly demonstrates that the LCS demarcate paths for the evolution of passively advected tracers.

To demonstrate the tidal contribution to stirring and mixing patterns in this region, the backward FTLEs are computed over a shorter time span (five days) based on the mean flow and actual tidal currents

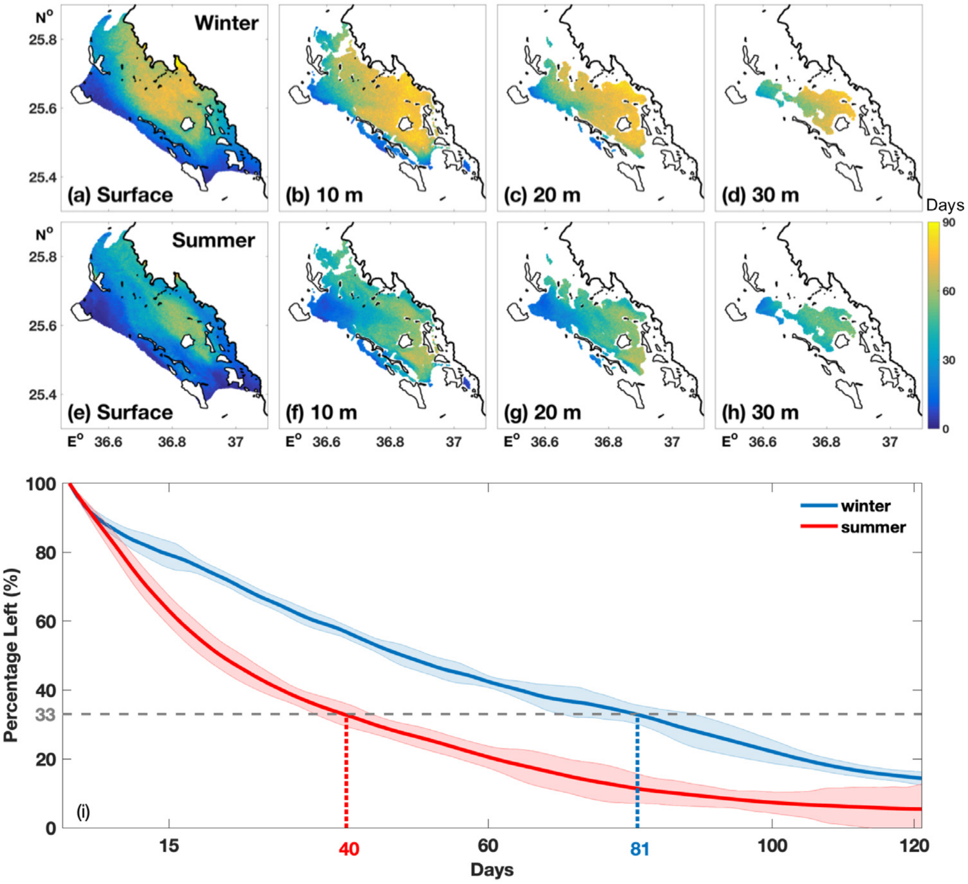

Fig. 7. Spatial distribution of RT (in days) at different layers estimated by particle releasing experiments. The RT is averaged from 60 experiments initiated on a daily basis in winter (a–d, February/March) and in summer (e–h, August/September). The color bar specifies the RT in days. (i) Time series of percentage of particles remaining inside the lagoon averaged over 60 experiments in which particles were subsequently released on an hourly basis. The blue and red lines represent particles released in winter (February/March) and summer (July/August) correspondingly. The error shading represents standard error statistically significant at the 95% confidence level.

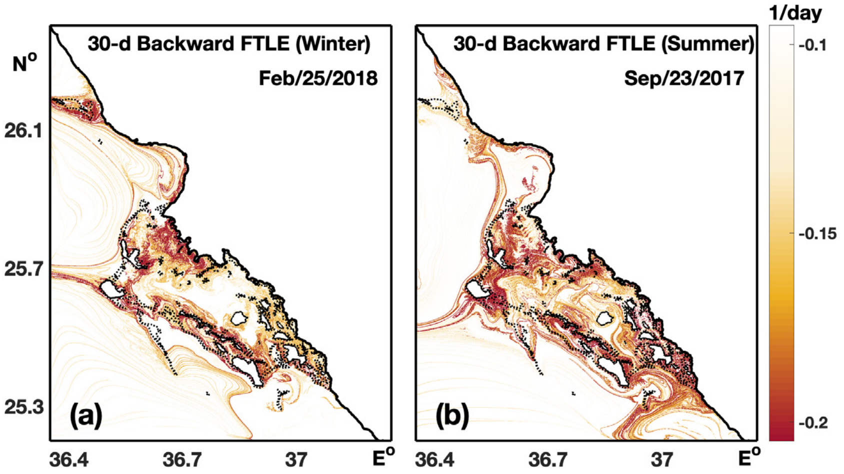

Fig. 8. FTLE in a winter month (a) and in a summer month (b). Each FTLE is computed with the daily averaged velocity fields over a 30-day period starting from the listed date backward in time. The color bar represents the magnitude of FTLE with units of $1/day$.

in August. Thirty experiments are carried out on a daily basis using ergodic tidal phases. Because the general tidal patterns, and not a particular flood or ebb event at a particular time, are of interest, the temporal average of the 30 FTLE fields computed using velocities with and without tides are shown in Fig. 10. In both scenarios, the currents appear to be impeded by the periphery of the reefs in the northern and western lagoon, as depicted by the dark ridges.

During a five-day period, the FTLE with tidal flow displays prominently higher intensity, particularly over the northern and western reef banks. For lagoons surrounded by shallow reef barriers, it is expected that water entering the lagoon during the flood tide does not penetrate far and remains near the reefs before exiting the lagoon after the reversed flood tidal currents (Andréfouët et al., 2006). Nevertheless, periodic tidal motions arise from exchanges with adjacent waters, and

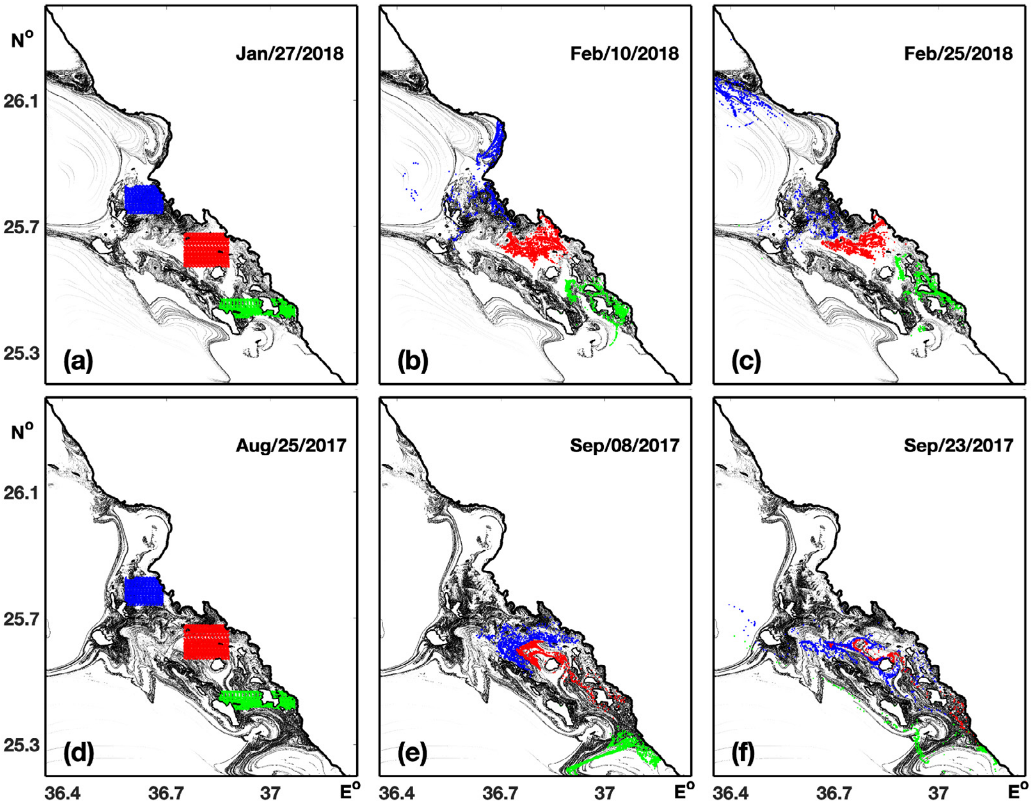

Fig. 9. Evolution of the locations of three sets of particles in the RSP lagoon during a 30-day period from January 27, 2018 to February 25, 2018 (a–c) and from August 25, 2017 to September 23, 2017 (d–f), superimposed on the spatial distributions of high values of the corresponding 30-day backward FTLE, as shown in Fig. 8.

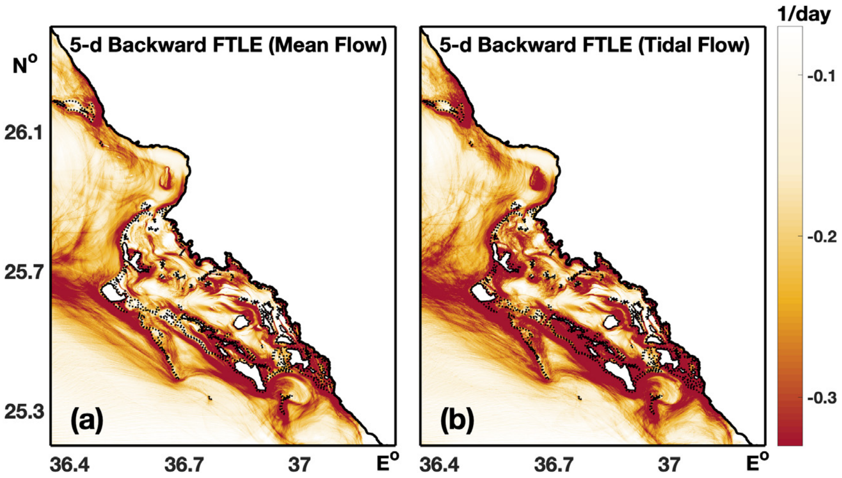

Fig. 10. Spatial distribution of temporally averaged backward FTLE (a) with the nontidal mean flow and (b) with the actual tidal flow. Each FTLE is computed with hourly velocity fields over a 5-day period started from 30 days in August 2017.

inlet jetting can result in rapid dispersion and attenuation of the tidal currents. This increases the chances of connectivity among nearby water regions, ultimately by sub-mesoscale or turbulent mixing over the ridges of the backward FTLE (Tartinville et al., 1997). Compared with the mean flow, the darker patches with tides suggest more active advection and stirring yielded by the tidal currents. Meanwhile, the coastal area appears to be insensitive to the tidal effect owing to its physical isolation from the lagoon edge because no obvious differences are observed in that area. In addition, strong background laminar flow to the southwest of the lagoon forms a clear northwest-to-southeast barrier, the location of which does not vary significantly with or without tides.

6. Summary

Based on the outputs of a high-resolution nested coastal model, the present study investigates the general circulation dynamics, water exchange, and their seasonal variabilities of the RSP lagoon in the Red Sea.

The physical processes controlling the circulation of a lagoon are primarily influenced by the lagoon size/topography, circulation dynamics of the adjacent sea, orientation to the prevailing wind direction, and tidal variability. The morphology of the surrounding shallow reef banks constrains the water exchange within the RSP lagoon and leads to a marked difference in water properties compared with the

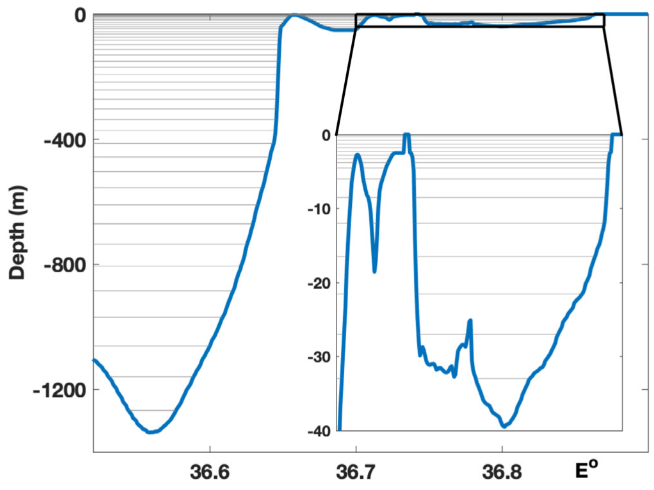

Fig. A.11. Spacing of vertical layers along the section indicated in Fig. 5(c).

adjacent sea. The area southwest of the lagoon is dominated by a northward boundary current throughout the year, a branch of which forms a retroflection that enters the lagoon from the northern inlets. The prevailing northwesterly wind regime persists throughout the year. However, an important feature of the local wind-driven currents, and one that may set it apart from the persistent winds, stems from the episodic jet events in wind forcing during winter. Significant changes in the wind speeds and directions caused by these strong jets result in rapid changes in the wind-driven circulation. The local wind-driven components include the direct downwind drift and upwind return flow at deeper layers. This happens in response to the wind-driven water level redistribution caused by the barotropic pressure gradient setup in the downwind direction. Meanwhile, the low-frequency rise and fall of the coastal sea level is controlled by the inflow and outflow produced by different wind regimes. Additional circulation caused by the water surface slope can arise from the water level variation outside the passes caused by tidal and wind effects over the shelf. Shelf tides force the exchange of water through the passages, with maximum velocities occurring over the western and southern shallow reef banks. The tidal currents are often dominant near the passages, whereas the interior circulation is primarily driven by wind forcing and long-term influence from the open sea, as well as partially adjusted by tidal rectification

Water exchange is largely limited by the reef barrier that surrounds the entire the RSP lagoon. The complex morphology slows down the water flow and increases the water flushing time, particularly in the central lagoon. In general, the lagoon water is likely to be ventilated more efficiently in summer with a significantly faster renewal rate than in winter. Near the reefs, the tidal currents of alternating inflow and outflow are often dominant, whereas in the interior, flow driven by the wind or currents from the open sea acts as the main ventilator of the semi-enclosed lagoon. Analysis of the particle trajectories and associated LCS patterns reveals distinct seasonality in the circulation patterns and RT. In winter, the water in the central lagoon is more weakly advected, with moderate exchange with the open sea. This could largely be attributed to wind jets in winter when water is pushed northwestward, which compensates for the southeastward currents. In summer, a large amount of water exits the lagoon from the southern outlets and the water exchange is more active with FTLE ridges aggregating throughout the lagoon.

This study presents the first investigation of the physical dynamics in the RSP lagoon to reveal the mechanisms that drive the unique circulation system and processes of water exchange under different scenarios. This can provide important insights into the circulation dynamics in similar coastal systems and serve as a benchmark for studying the ecosystems in those environments.

CRediT authorship contribution statement

Peng Zhan: Conceptualization, Methodology, Writing - original draft, Validation, Investigation, Formal analysis, Visualization, Software. **George Krokos:** Conceptualization. **Sabique Langodan:** Validation, Resources. **Daquan Guo:** Conceptualization, Software. **Hari Dasari:** Validation, Resources. **Vassilis P. Papadopoulos:** Resources, Writing - review & editing. **Pierre F.J. Lermusiaux:** Methodology. **Omar M. Knio:** Methodology. **Ibrahim Hoteit:** Conceptualization, Supervision, Writing - review & editing.

Declaration of competing interest

The authors declare that they have no known competing financial interests or personal relationships that could have appeared to influence the work reported in this paper.

Acknowledgments

The research was supported by the Office of Sponsor Research (OSR) at King Abdullah University of Science and Technology (KAUST), Saudi Arabia under the Virtual Red Sea Initiative (grant no. REP/1/3268-01-01), by the Saudi Aramco Marine Environment Research Center at KAUST, Saudi Arabia, and the Beacon Development Company, Saudi Arabia. All model runs are conducted on the KAUST supercomputing facility SHAHEEN.

Appendix A. Vertical grid spacing

A high vertical resolution vertical grid is configured in z-coordinate to resolve the steep topography (Fig. A.11). Specifically, the model is implemented with 50 vertical layers, with the upper 4 m equally divided into 8 layers (thickness of each layer = 0.5 m) to resolve the shallow coral complex and fringing reefs, and the upper 40 m is divided into 18 layers to resolve the steep topography at the reef edges and inside the lagoon.

Appendix B. Computing the FTLE

The LCS can be identified as the ridges of the FTLE fields (Shadden et al., 2005). FTLE is a scalar quantity that represents the rate of separation of initially neighboring particles over a finite-time window $[t, t+T]$. Considering an arbitrary point $\mathbf{x}_t$ at time t, at each location of the studied domain, the FTLE represents the growth factor of the norm of a perturbation $\delta\mathbf{x}_t$ that started at time t and advected by the flow after an advection time T. Maximal stretching occurs when $\delta\mathbf{x}_t$ is aligned with the eigenvector associated with the largest eigenvalue λ_{max} of the Cauchy–Green deformation tensor $\Delta = \mathbf{M}^T\mathbf{M}$, where $\mathbf{M} : \mathbf{x}_t \mapsto \mathbf{x}_{t+T}$ is the flow map that advances points $\mathbf{x}_t$ in the domain at time t to their new locations $\mathbf{x}_{t+T}$ at time $t+T$. The backward FTLE (i.e., $T < 0$) is then defined as $FTLE = log(\lambda_{max})/2T$. The readers are referred to Haller (2015) for more details about the computation of the FTLE discussed above.

References

Andréfouët, S., Ouillon, S., Brinkman, R., Falter, J., Douillet, P., Wolk, F., Smith, R., Garen, P., Martinez, E., Laurent, V., Lo, C., Remoissenet, G., Scourzic, B., Gilbert, A., Deleersnijder, E., Steinberg, C., Choukroun, S., Buestel, D., 2006. Review of solutions for 3D hydrodynamic modeling applied to aquaculture in South Pacific atoll lagoons. Mar. Pollut. Bull. http://dx.doi.org/10.1016/j.marpolbul.2006.07.014.

Andrews, J.C., 1990. The physical oceanography of coral-reef systems. Coral Reefs Ecosyst. World 25, 11–48.

Balotro, R.S., Isobe, A., Shimizu, M., 2003. Seasonal variability in circulation pattern and residence time of Suo-Nada. J. Oceanogr. http://dx.doi.org/10.1023/A:1025555608384.

Beron-Vera, F.J., Olascoaga, M.J., 2009. An assessment of the importance of chaotic stirring and turbulent mixing on the West Florida shelf. J. Phys. Oceanogr. http://dx.doi.org/10.1175/2009JPO4046.1.

Beron-Vera, F.J., Olascoaga, M.J., Goni, G.J., 2010. Surface ocean mixing inferred from different multisatellite altimetry measurements. J. Phys. Oceanogr. http://dx.doi.org/10.1175/2010JPO4458.1.

Bettencourt, J.H., López, C., Hernández-García, E., 2012. Oceanic three-dimensional Lagrangian coherent structures: A study of a mesoscale eddy in the Benguela upwelling region. Ocean Model. http://dx.doi.org/10.1016/j.ocemod.2012.04.004, arXiv:1111.3792.

Calil, P.H., Richards, K.J., 2010. Transient upwelling hot spots in the oligotrophic North Pacific. J. Geophys. Res.: Oceans http://dx.doi.org/10.1029/2009JC005360.

Carvalho, S., Aylagas, E., Villalobos, R., Kattan, Y., Berumen, M., Pearman, J.K., 2019. Beyond the visual: Using metabarcoding to characterize the hidden reef cryptobiome. Proc. R. Soc. B: Biol. Sci. http://dx.doi.org/10.1098/rspb.2018.2697.

Cavalcante, G.H., Kjerfve, B., Feary, D.A., 2012. Examination of residence time and its relevance to water quality within a coastal mega-structure: The Palm Jumeirah Lagoon. J. Hydrol. http://dx.doi.org/10.1016/j.jhydrol.2012.08.027.

Cerralbo, P., Espino, M., Grifoll, M., 2016. Modeling circulation patterns induced by spatial cross-shore wind variability in a small-size coastal embayment. Ocean Model. http://dx.doi.org/10.1016/j.ocemod.2016.05.011.

Chao, Y., Li, Z., Farrara, J.D., Hung, P., 2009. Blending sea surface temperatures from multiple satellites and in situ observations for coastal oceans. J. Atmos. Ocean. Technol. http://dx.doi.org/10.1175/2009JTECHO592.1.

Chapman, D.C., Giese, G.S., 2019. Seiches. In: Encyclopedia of Ocean Sciences. http://dx.doi.org/10.1016/B978-0-12-409548-9.10824-3.

Csanady, G.T., 1982. Circulation in the coastal ocean. Circ. Coast. Ocean http://dx.doi.org/10.1029/eo064i046p00933-01.

Dee, D.P., Uppala, S.M., Simmons, A.J., Berrisford, P., Poli, P., Kobayashi, S., Andrae, U., Balmaseda, M.A., Balsamo, G., Bauer, P., Bechtold, P., Beljaars, A.C., van de Berg, L., Bidlot, J., Bormann, N., Delsol, C., Dragani, R., Fuentes, M., Geer, A.J., Haimberger, L., Healy, S.B., Hersbach, H., Hólm, E.V., Isaksen, L., Kållberg, P., Köhler, M., Matricardi, M., Mcnally, A.P., Monge-Sanz, B.M., Morcrette, J.J., Park, B.K., Peubey, C., de Rosnay, P., Tavolato, C., Thépaut, J.N., Vitart, F., 2011. The ERA-Interim reanalysis: Configuration and performance of the data assimilation system. Q. J. R. Meteorol. Soc. http://dx.doi.org/10.1002/qj.828.

Doshi, M., Kulkarni, C.S., Ali, W.H., Gupta, A., Lermusiaux, P.F., Zhan, P., Hoteit, I., Knio, O., 2019. Flow maps and coherent sets for characterizing residence times and connectivity in lagoons and coral reefs: the case of the red sea. In: OCEANS 2019 MTS/IEEE SEATTLE. IEEE, pp. 1–8. http://dx.doi.org/10.23919/OCEANS40490.2019.8962643.

D'Ovidio, F., Fernández, V., Hernández-García, E., López, C., 2004. Mixing structures in the Mediterranean Sea from finite-size Lyapunov exponents. Geophys. Res. Lett. http://dx.doi.org/10.1029/2004GL020328, arXiv:0404041.

Duran, R., Beron-Vera, F.J., Olascoaga, M.J., 2018. Extracting quasi-steady Lagrangian transport patterns from the ocean circulation: An application to the Gulf of Mexico. Sci. Rep. http://dx.doi.org/10.1038/s41598-018-23121-y.

Egbert, G.D., Bennett, A.F., Foreman, M.G.G., 1994. TOPEX/POSEIDON tides estimated using a global inverse model. J. Geophys. Res.: Oceans 99 (C12), 24821–24852. http://dx.doi.org/10.1029/94JC01894.

Fiorentino, L.A., Olascoaga, M.J., Reniers, A., Feng, Z., Beron-Vera, F.J., MacMahan, J.H., 2012. Using Lagrangian Coherent Structures to understand coastal water quality. Cont. Shelf Res. http://dx.doi.org/10.1016/j.csr.2012.07.009.

Georgiou, S., Ypma, S.L., Brüggemann, N., Sayol, J.M., Pietrzak, J.D., Katsman, C.A., 2020. Pathways of the water masses exiting the Labrador Sea: The importance of boundary–interior exchanges. Ocean Model. http://dx.doi.org/10.1016/j.ocemod.2020.101623.

Gill, A.E., 1982. Atmosphere - Ocean Dynamics. Academic Press Inc., New York, U.S.A., http://dx.doi.org/10.1016/0141-1187(83)90039-1.

Gough, M.K., Beron-Vera, F.J., Olascoaga, M.J., Sheinbaum, J., Jouanno, J., Duran, R., 2019. Persistent Lagrangian transport patterns in the northwestern Gulf of Mexico. J. Phys. Oceanogr. http://dx.doi.org/10.1175/JPO-D-17-0207.1, arXiv:1710.04027.

Griffies, S.M., Hallberg, R.W., 2000. Biharmonic friction with a Smagorinsky-like viscosity for use in large-scale eddy-permitting ocean models. Mon. Weather Rev. http://dx.doi.org/10.1175/1520-0493(2000)128<2935:bfwasl>2.0.co;2.

Guo, D., Akylas, T.R., Zhan, P., Kartadikaria, A., Hoteit, I., 2016. On the generation and evolution of internal solitary waves in the southern Red Sea. J. Geophys. Res.: Oceans http://dx.doi.org/10.1002/2016JC012221.

Guo, D., Zhan, P., Hoteit, I., 2021. Three-dimensional simulation of shoaling internal solitary waves and their influence on particle transport in the southern red sea. J. Geophys. Res.: Oceans http://dx.doi.org/10.1029/2020JC016335.

Haller, G., 2015. Lagrangian Coherent structures. Annu. Rev. Fluid Mech. 47 (1), 137–162. http://dx.doi.org/10.1146/annurev-fluid-010313-141322.

Haza, A.C., Özgökmen, T.M., Hogan, P., 2016. Impact of submesoscales on surface material distribution in a gulf of Mexico mesoscale eddy. Ocean Model. http://dx.doi.org/10.1016/j.ocemod.2016.10.002.

Hernández-Carrasco, I., López, C., Orfila, A., Hernández-García, E., 2013. Lagrangian Transport in a microtidal coastal area: The Bay of Palma, island of Mallorca, Spain. Nonlinear Process. Geophys. http://dx.doi.org/10.5194/npg-20-921-2013.

Hoteit, I., Abualnaja, Y., Afzal, S., Ait-El-Fquih, B., Akylas, T., Antony, C., Dawson, C., Asfahani, K., Brewin, R.J., Cavaleri, L., Cerovecki, I., Cornuelle, B., Desamsetti, S., Attada, R., Dasari, H., Sanchez-Garrido, J., Genevier, L., Gharamti, M.E., Gittings, J.A., Gokul, E., Gopalakrishnan, G., Guo, D., Hadri, B., Hadwiger, M., Hammoud, M.A., Hendershott, M., Hittawe, M., Karumuri, A., Knio, O., KÃűhl, A., Kortas, S., Krokos, G., Kunchala, R., Issa, L., Lakkis, I., Langodan, S., Lermusiaux, P., Luong, T., Ma, J., Maitre, O.L., Mazloff, M., Mohtar, S.E., Papadopoulos, V.P., Platt, T., Pratt, L., Raboudi, N., Racault, M.-F., Raitsos, D.E., Razak, S., Sanikommu, S., Sathyendranath, S., Sofianos, S., Subramanian, A., Sun, R., Titi, E., Toye, H., Triantafyllou, G., Tsiaras, K., Vasou, P., Viswanadhapalli, Y., Wang, Y., Yao, F., Zhan, P., Zodiatis, G., 2021. Towards an end-to-end analysis and prediction system for weather, climate, and marine applications in the red sea. Bulletin of the American Meteorological Society 102 (1), E99 – E122. http://dx.doi.org/10.1175/BAMS-D-19-0005.1.

Huhn, F., von Kameke, A., Allen-Perkins, S., Montero, P., Venancio, A., Pérez-Muñuzuri, V., 2012. Horizontal Lagrangian transport in a tidal-driven estuary-Transport barriers attached to prominent coastal boundaries. Cont. Shelf Res. http://dx.doi.org/10.1016/j.csr.2012.03.005.

Ioc, I., 2008. Centenary Edition of the GEBCO Digital Atlas, Published on CD-ROM on behalf of the Intergovernmental Oceanographic Commission and the International Hydrographic Organization as part of the General Bathymetric Chart of the Oceans. BODC, 2003, British Oceanographic Data Centre, Liverpool.

Jiang, H.S., Farrar, T., Beardsley, R.C., Chen, R., Chen, C.S., 2009. Zonal surface wind jets across the Red Sea due to mountain gap forcing along both sides of the Red Sea. Geophys. Res. Lett. 36, http://dx.doi.org/10.1029/2009gl040008, Artn L19605.

Kraines, S.B., Yanagi, T., Isobe, M., Komiyama, H., 1998. Wind-wave driven circulation on the coral reef at Bora Bay, Miyako Island. Coral Reefs http://dx.doi.org/10.1007/s003380050107.

Langodan, S., Cavaleri, L., Pomaro, A., Vishwanadhapalli, Y., Bertotti, L., Hoteit, I., 2017a. The climatology of the Red Sea – part 2: the waves. Int. J. Climatol. http://dx.doi.org/10.1002/joc.5101.

Langodan, S., Cavaleri, L., Vishwanadhapalli, Y., Pomaro, A., Bertotti, L., Hoteit, I., 2017b. The climatology of the Red Sea – part 1: the wind. Int. J. Climatol. http://dx.doi.org/10.1002/joc.5103.

Large, W.G., McWilliams, J.C., Doney, S.C., 1994. Oceanic vertical mixing: A review and a model with a nonlocal boundary layer parameterization. Rev. Geophys. http://dx.doi.org/10.1029/94RG01872.

Lehahn, Y., D'Ovidio, F., Lévy, M., Heifetz, E., 2007. Stirring of the northeast Atlantic spring bloom: A Lagrangian analysis based on multisatellite data. J. Geophys. Res.: Oceans 112 (C8), http://dx.doi.org/10.1029/2006JC003927.

Lekien, F., Coulliette, C., Mariano, A.J., Ryan, E.H., Shay, L.K., Haller, G., Marsden, J., 2005. Pollution release tied to invariant manifolds: A case study for the coast of Florida. Physica D http://dx.doi.org/10.1016/j.physd.2005.06.023.

Lentz, S.J., Churchill, J.H., Davis, K.A., Farrar, J.T., 2016a. Surface gravity wave transformation across a platform coral reef in the Red Sea. J. Geophys. Res.: Oceans http://dx.doi.org/10.1002/2015JC011142.

Lentz, S.J., Churchill, J.H., Davis, K.A., Farrar, J.T., Pineda, J., Starczak, V., 2016b. The characteristics and dynamics of wave-driven flow across a platform coral reef in the Red Sea. J. Geophys. Res.: Oceans http://dx.doi.org/10.1002/2015JC011141.

Lentz, S.J., Davis, K.A., Churchill, J.H., DeCarlo, T.M., 2017. Coral reef drag coefficients - Water depth dependence. J. Phys. Oceanogr. http://dx.doi.org/10.1175/JPO-D-16-0248.1.

Lindo-Atichati, D., Curcic, M., Paris, C.B., Buston, P.M., 2016. Description of surface transport in the region of the Belizean Barrier reef based on observations and alternative high-resolution models. Ocean Model. http://dx.doi.org/10.1016/j.ocemod.2016.09.010.

Lowe, R.J., Falter, J.L., Monismith, S.G., Atkinson, M.J., 2009. A numerical study of circulation in a coastal reef-lagoon system. J. Geophys. Res.: Oceans http://dx.doi.org/10.1029/2008JC005081.

Lugo-Fernández, A., Roberts, H.H., Wiseman, W.J., 2004. Currents, water levels, and mass transport over a modern Caribbean coral reef: Tague Reef, St. Croix, USVI. Cont. Shelf Res. http://dx.doi.org/10.1016/j.csr.2004.07.004.

Madah, F., Mayerle, R., Bruss, G., Bento, J., 2015. Characteristics of tides in the Red Sea region, a numerical model study. Open J. Mar. Sci. http://dx.doi.org/10.4236/ojms.2015.52016.

Marshall, J., Hill, C., Perelman, L., Adcroft, A., 1997. Hydrostatic, quasi-hydrostatic, and nonhydrostatic ocean modeling. J. Geophys. Res. 102 (C3), 5733. http://dx.doi.org/10.1029/96JC02776.

Mathieu, P.P., Deleersnijder, E., Cushman-Roisin, B., Beckers, J.M., Bolding, K., 2002. The role of topography in small well-mixed bays, with application to the lagoon of Mururoa. Cont. Shelf Res. http://dx.doi.org/10.1016/S0278-4343(02)00002-X.

Monismith, S.G., Genin, A., Reidenbach, M.A., Yahel, G., Koseff, J.R., 2006. Thermally driven exchanges between a coral reef and the adjoining ocean. J. Phys. Oceanogr. http://dx.doi.org/10.1175/JPO2916.1.

Monsen, N.E., Cloern, J.E., Lucas, L.V., Monismith, S.G., 2002. A comment on the use of flushing time, residence time, and age as transport time scales. Limnol. Oceanogr. http://dx.doi.org/10.4319/lo.2002.47.5.1545.

Montaño-Ley, Y., Soto-Jiménez, M.F., 2019. A numerical investigation of the influence time distribution in a shallow coastal lagoon environment of the Gulf of California. Environ. Fluid Mech. http://dx.doi.org/10.1007/s10652-018-9619-3.

Nanninga, G.B., Saenz-Agudelo, P., Zhan, P., Hoteit, I., Berumen, M.L., 2015. Not finding Nemo: limited reef-scale retention in a coral reef fish. Coral Reefs 34 (2), 383–392. http://dx.doi.org/10.1007/s00338-015-1266-2.

Nencioli, F., D'Ovidio, F., Doglioli, A.M., Petrenko, A.A., 2011. Surface coastal circulation patterns by in-situ detection of Lagrangian coherent structures. Geophys. Res. Lett. http://dx.doi.org/10.1029/2011GL048815.

Olascoaga, M.J., Beron-Vera, F.J., Brand, L.E., Koçak, H., 2008. Tracing the early development of harmful algal blooms on the West Florida Shelf with the aid of Lagrangian coherent structures. J. Geophys. Res.: Oceans http://dx.doi.org/10.1029/2007JC004533.

Olascoaga, M.J., Rypina, I.I., Brown, M.G., Beron-Vera, F.J., Koçak, H., Brand, L.E., Halliwell, G.R., Shay, L.K., 2006. Persistent transport barrier on the West Florida Shelf. Geophys. Res. Lett. http://dx.doi.org/10.1029/2006GL027800.

Oliveira, A.M., Kjerfve, B., 1993. Environmental responses of a tropical coastal lagoon system to hydrological variability: Mundaú-Manguaba, Brazil. Estuar. Coast. Shelf Sci. http://dx.doi.org/10.1006/ecss.1993.1074.

Ottino, J.M., 1989. The kinematics of mixing: stretching, chaos, and transport.

Paris, C.B., Helgers, J., van Sebille, E., Srinivasan, A., 2013. Connectivity Modeling System: A probabilistic modeling tool for the multi-scale tracking of biotic and abiotic variability in the ocean. Environ. Modell. Softw. http://dx.doi.org/10.1016/j.envsoft.2012.12.006.

Peacock, T., Dabiri, J., 2010. Introduction to focus issue: Lagrangian coherent structures. Chaos http://dx.doi.org/10.1063/1.3278173.

Raitsos, D.E., Brewin, R.J., Zhan, P., Dreano, D., Pradhan, Y., Nanninga, G.B., Hoteit, I., 2017. Sensing coral reef connectivity pathways from space. Sci. Rep. http://dx.doi.org/10.1038/s41598-017-08729-w.

Shadden, S.C., Lekien, F., Marsden, J.E., 2005. Definition and properties of Lagrangian coherent structures from finite-time Lyapunov exponents in two-dimensional aperiodic flows. Physica D http://dx.doi.org/10.1016/j.physd.2005.10.007.

Symonds, G., Black, K.P., Young, I.R., 1995. Wave-driven flow over shallow reefs. J. Geophys. Res. http://dx.doi.org/10.1029/94JC02736.

Tartinville, B., Deleersnijder, E., Rancher, J., 1997. The water residence time in the Mururoa atoll lagoon: Sensitivity analysis of a three-dimensional model. Coral Reefs http://dx.doi.org/10.1007/s003380050074.

Toye, H., Zhan, P., Gopalakrishnan, G., Kartadikaria, A.R., Huang, H., Knio, O., Hoteit, I., 2017. Ensemble data assimilation in the Red Sea: sensitivity to ensemble selection and atmospheric forcing. Ocean Dyn. http://dx.doi.org/10.1007/s10236-017-1064-1.

Umgiesser, G., Ferrarin, C., Cucco, A., De Pascalis, F., Bellafiore, D., Ghezzo, M., Bajo, M., 2014. Comparative hydrodynamics of 10 mediterranean lagoons by means of numerical modeling. J. Geophys. Res.: Oceans http://dx.doi.org/10.1002/2013JC009512.

Viswanadhapalli, Y., Dasari, H.P., Langodan, S., Challa, V.S., Hoteit, I., 2017. Climatic features of the Red Sea from a regional assimilative model. Int. J. Climatol. http://dx.doi.org/10.1002/joc.4865.

Wang, Y., Raitsos, D.E., Krokos, G., Gittings, J.A., Zhan, P., Hoteit, I., 2019. Physical connectivity simulations reveal dynamic linkages between coral reefs in the southern Red Sea and the Indian Ocean. Sci. Rep. 9 (1), 1–11.

Yahel, G., Post, A.F., Fabricius, K., Marie, D., Vaulot, D., Genin, A., 1998. Phytoplankton distribution and grazing near coral reefs. Limnol. Oceanogr. http://dx.doi.org/10.4319/lo.1998.43.4.0551.

Yao, F., Hoteit, I., Pratt, L.J., Bower, A.S., Köhl, A., Gopalakrishnan, G., Rivas, D., 2014a. Seasonal overturning circulation in the Red Sea. 2: Winter circulation. J. Geophys. Res.: Oceans 2263–2289. http://dx.doi.org/10.1002/2013JC009331.

Yao, F., Hoteit, I., Pratt, L.J., Bower, A.S., Zhai, P., Köhl, A., Gopalakrishnan, G., 2014b. Seasonal overturning circulation in the Red Sea: 1. Model validation and summer circulation. J. Geophys. Res.: Oceans 2238–2262. http://dx.doi.org/10.1002/2013JC009004.

Zhan, P., Gopalakrishnan, G., Subramanian, A.C., Guo, D., Hoteit, I., 2018. Sensitivity studies of the Red Sea eddies using adjoint method. J. Geophys. Res.: Oceans (ja), http://dx.doi.org/10.1029/2018JC014531, URL: https://agupubs.onlinelibrary.wiley.com/doi/abs/10.1029/2018JC014531.

Zhan, P., Krokos, G., Guo, D., Hoteit, I., 2019. Three-dimensional signature of the Red Sea eddies and eddy-induced transport. Geophys. Res. Lett. 46 (4), 2167–2177. http://dx.doi.org/10.1029/2018GL081387.

Zhan, P., Subramanian, A.C., Yao, F., Hoteit, I., 2014. Eddies in the Red Sea: A statistical and dynamical study. J. Geophys. Res.: Oceans 119 (6), 3909–3925. http://dx.doi.org/10.1002/2013JC009563.

Zhan, P., Subramanian, A.C., Yao, F., Kartadikaria, A.R., Guo, D., Hoteit, I., 2016. The eddy kinetic energy budget in the Red Sea. J. Geophys. Res.: Oceans 121 (7), 4732–4747. http://dx.doi.org/10.1002/2015JC011589.

Zhan, P., Yao, F., Kartadikaria, A.R., Viswanadhapalli, Y., Gopalakrishnan, G., Hoteit, I., 2015. Far-field ocean conditions and concentrate discharges modeling along the saudi coast of the red sea. In: Missimer, T.M., Jones, B., Maliva, R.G. (Eds.), Intakes and Outfalls for Seawater Reverse-Osmosis Desalination Facilities: Innovations and Environmental Impacts. Springer International Publishing, Cham, pp. 501–520. http://dx.doi.org/10.1007/978-3-319-13203-7_21.